www.lajss.org
Latin American Journal of Solids and Structures 1 (2004) 185–218

An anisotropic continuum damage model: Theory and numerical analyses

Michael Brünig

Lehrstuhl für Baumechanik - Statik, Universität Dortmund,
August-Schmidt-Str. 6, D-44221 Dortmund, Germany

Abstract

The overview paper deals with fundamental constitutive issues in the elastic-plastic-damage rate theory and numerical analyses of the large strain elastic-plastic deformation behavior of anisotropically damaged ductile metals. The proposed model is based on a generalized macroscopic theory within the framework of nonlinear continuum damage mechanics taking into account kinematic description of damage. It employs the consideration of damaged as well as fictitious undamaged configurations related via metric transformations. To be able to address both the plastic flow and the anisotropic damage process, respective Helmholtz free energy functions of the fictitious undamaged configuration and of the current damaged configuration as well as a generalized yield condition and a damage criterion are introduced separately. The evolution laws for plastic and damage strains are based on numerous experimental observations and numerical calculations at the micro-level. Identification of material parameters is discussed in some detail. The applicability of the proposed continuum damage theory is demonstrated by numerical simulation of the inelastic deformation process of tension specimens.

Keywords: Elastic-plastic metals, Anisotropic ductile damage, Voids and micro-cracks, Finite strains.

1 Introduction

The accurate and realistic description of inelastic behavior of ductile metals is essential for the solution of numerous boundary-value problems occurring in various engineering fields. For example, microscopic defects and cracks cause reduction in strength of materials and shorten the life time of engineering structures. Therefore, a main issue in engineering applications is to provide realistic information on the stress distribution within elements of such materials or assessment of safety factor against failure. It is well known that large inelastic deformations of polycrystalline materials caused by dislocations along preferred slip planes are usually accompanied by certain damage processes due to microdefects like microvoids, microcracks, and micro-shearbands.

* Corresp. author: michael.bruenig@uni-dortmund.de Received 27 Feb 2004; In revised form 26 March 2004

These damage processes may start at a certain stage of the deformation process and result in the development of macrodefects leading to rupture. Thus, proper understanding and mechanical description of the damage process caused by internal defects are of importance in discussing the mechanical effects of material deterioration on the macroscopic behavior of materials as well as in elucidating the process leading from these defects to final fracture.

Therefore, the phenomenon of initiation and growth of cavities and microcracks induced by large deformations in metals has been extensively studied by means of micromechanical analyses. McClintock [65] and Rice and Tracey [77] presented first micromechanical studies of the growth of a single void in an infinite elastic-plastic solid and the results were used to estimate critical strains for void coalescence. Needleman [71] analyzed an elastic-plastic medium containing a doubly periodic square array of voids takig into account void interaction effects. His results predicted smaller critical strains than those obtained by single void models [65, 77]. In addition, a porous ductile material model has been developed by Gurson [34] using a characteristic volume element consisting of an aggregate of voids and rigid plastic matrix material. Improvements of this model are given by Tvergaard [87] based on systematic numerical analyses on the microscale. The continuum mechanical overall effect of those defects is derived by homogenization [7, 45, 47]. Although at the microscale a good representation of physical mechanisms can be reached, difficulties arise when these models have to be included in large scale analyses to predict failure due to the lack of accuracy of local stress calculations for the microscale level. Thus, a systematic approach to the problems of distributed defects has to be provided which constitutes a practical tool to take into account the various damaging processes in materials and structures at a macroscopic continuum level.

To be able to describe the gradual internal deterioration of solids within the framework of continuum thermodynamics several continuum damage models have been proposed which are either phenomenological or micromechanically based. Within these concepts the material behavior is modeled by constitutive equations taking into account its progressive deterioration and, therefore, may be seen as a complementary tool between continuum mechanics and fracture mechanics. In particular, the fundamental notion of continuum damage mechanics is attributed originally to Kachanov [41] and was modified by Rabotnov [76] based on the concept of effective stress in damaged materials. Afterwards, in order to describe the accumulative material degradation by means of continuous field variables continuum damage mechanics has become an emerging field of active research. During the past decades the constitutive modelling of ductile damaged materials in the finite deformation range has received considerable attention, as can be seen from a large number of bibliographies, reviews and discussions [23, 24, 46, 57, 87, 90]. The predictive utility of an appropriate damage model strongly depends on its particular choice of the damage variable. As a result of the arbitrary nature of the choice of internal variables, however, the current literature discusses many ways to phenomenologically define or micromechanically derive damage variables representing the state of internal deterioration of the material properties and, hence, different and often contradictory models have been proposed [4, 46].

Continuum damage mechanics discusses systematically the effects of damage on the mechan-

ical properties of materials and structures as well as the influence of external conditions and damage itself on the subsequent development of damage. Critical values of proposed continuous damage variables may be viewed as major parameters characterizing the onset of failure. Therefore, an important issue in such phenomenological constitutive models is the appropriate choice of the physical nature of mechanical variables realistically describing the damage state of materials and their tensorial representation. For example, scalar valued damage variables have been proposed [2, 29, 41, 54, 55, 58, 76, 78, 85] and have successfully been employed in some practical applications [31, 32, 38]. Although the simplicity and efficiency of a scalar damage representation is indeed very attractive, the orientation-independent isotropic damage variable is subsequently found to be inaccurate as there is strong experimental evidence that damage in the form of planar microvoids usually nucleates and grows on grain boundaries whose planes are perpendicular to the maximum tensile stress direction [68, 73]. It has been shown that the nucleation and growth of voids as well as the orientation of fissures and their lengths observed in the process of material damage depend significantly on the direction of the applied stresses or strains and, hence, damage is in general anisotropic. Chow and Wang [25, 26] reported that isotropic damage models usually predict lower strength of materials compared to the theory of anisotropic damage, and the importance of the directional nature of material damage in controlling final rupture becomes more pronounced under non-proportional loading conditions. An analysis without taking into account the damage-induced material anisotropy may therefore lead to questionable results.

Thus, axial vector representations have been proposed [44, 48, 49] and second order damage tensors [4, 9, 10, 17–21, 25, 40, 42, 44, 61, 70, 84, 89], as well as higher order damage tensors [22] have been introduced in order to adequately describe anisotropic damage phenomena. Hence, different choices are based on assumptions a priori made on the microstructure level according to the level of simplification of the model. Furthermore, efforts have been made to develop theories of ductile fracture based upon the nucleation and growth of voids during straining and upon plastic flow localization into narrow bands within the deforming porous regions which then become the sites of macrofracture development. An overview and classification of available models in local approach of fracture are given by Lemaitre [56]. Hence, accurate and efficient constitutive models of damaged ductile materials are needed as the basis for an accurate theory of ductile fracture.

The applicability of an accurate material model requires specification of the significant macroscopic and microscopic features of the material structure. It has been observed in metallurgical tests that nucleation of microvoids and their growth and coalescence are the main steps toward the formation of a mesocrack in ductile materials, which eventually leads to failure. For example, while the statistical nature of void formation results in cavities being nucleated over a range of strains, void nucleation in most alloys begins early in the deformation process and, as a result, the damage and fracture behavior is controlled by void growth and void link-up. This behavior affects various local and averaged material properties such as the elastic constitutive parameters [58]. These property changes are indicative of material degradation, and

their measurement can be used to determine appropriate damage variables in engineering materials. For example, the variation of elastic properties has been proposed as an appropriate measure of damage [4, 58, 75] which is experimentally realizable due to its clearly identifiable meaning. Chaboche [23] discussed different ways to define the damage variable through indirect measurement procedures and each interpretation of damage requires a corresponding model. In addition, Alves et al. [1, 2] reported of some damage measurements using different experimental techniques. Their results indicate different values for the damage parameters on the same specimen according to the definition of damage and to the experimental technique employed and, therefore, damage is an adjustable parameter. Thus, the choice of the most appropriate damage measure is not an easy task and the damage parameter determined experimentally must be carefully related to the theoretical model.

In order to develop an elaborate continuum damage theory for the inelastic behavior of ductile metals, a systematic macroscopic framework is established for describing the coupled processes of elastic, plastic and damage deformations of anisotropic nature. Based on the concepts of continuum damage mechanics constitutive equations for ductile engineering materials are discussed in the present overview by introducing a limited number of state parameters. Thus, a general anisotropic damage evolution model is proposed and satisfactorily verified by experimental results and microscopic numerical analyses reported in the literature. Briefly, the present anisotropic elastic-plastic-damage framework is based on the introduction of metric transformation tensors. The kinematic description employs the consideration of damaged as well as fictitious undamaged configurations and the introduction of corresponding Helmholtz free energy functions. Therefore, the model does not need strain equivalence, stress equivalence or strain energy equivalence approaches often used in continuum damage theories to be able to connect matrix material and aggregate variables [25, 54, 55, 79, 80, 89]. The damaged and corresponding undamaged configurations are related via metric transformations which allow for the interpretation of damage tensors. Therefore, a characteristic feature of the proposed model is the kinematic description of anisotropic damage. The modular structure is accomplished by the kinematic decomposition of strain rates into elastic, plastic and damage parts which take into account the physics of these deformation processes. To be able to address equally the two physically distinct modes of irreversible changes a generalized macroscopic yield condition and a damage surface are formulated separately. The evolution laws for plastic and damage strain rates are based on numerous experimental observations and numerical calculations at the microlevel. Identification of material parameters is discussed and the applicability of the present continuum damage theory is demonstrated by numerical analyses of the inelastic damage process of specimens undergoing tensile loading. The influence of different model parameters on the deformation and failure behavior of ductile metals is studied in some detail and the numerical results are compared with available experimental data.

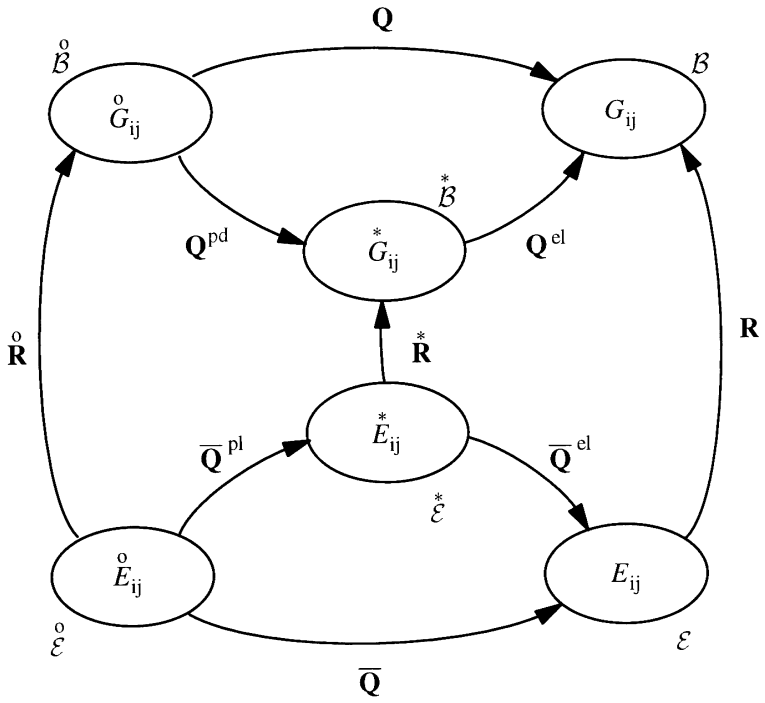

Figure 1: Configurations, metrics, and metric transformation tensors.

2 Kinematics

The kinematic framework presented by Brünig [18] is used to describe inelastic deformation behavior of anisotropically damaged solids. Briefly, the continuous body in the predamaged but undeformed initial configuration $\overset{o}{\mathcal{B}}$ is shown in Figure 1. Tensorial quantities referred to this configuration are formulated using the base vectors $\overset{o}{\mathbf{g}}_i$ and the associated metric coefficients are given by $\overset{o}{G}_{ij}=\overset{o}{\mathbf{g}}_i \cdot \overset{o}{\mathbf{g}}_j$. In addition, the current elastic-plastically deformed and damaged configuration $\mathcal{B}$ is considered and the corresponding base vectors and metric coefficients are $\mathbf{g}_i$ and $G_{ij} = \mathbf{g}_i \cdot \mathbf{g}_j$, respectively (see Fig. 1). All actual quantities are referred to this current damaged configuration.

The kinematic theory for the mechanics of large deformations of solids is based on the metric transformation tensor [15, 17, 52, 53]

$$\mathbf{Q} = Q^i_{.j}\, \mathbf{g}_i \otimes \mathbf{g}^j = \overset{o}{G}{}^{ik}\, G_{kj}\, \mathbf{g}_i \otimes \mathbf{g}^j \tag{1}$$

which is used to define the logarithmic Hencky strain tensor

$$\mathbf{A} = \frac{1}{2} \ln\mathbf{Q} = \frac{1}{2} (\ln Q)^i_{.j}\, \mathbf{g}_i \otimes \mathbf{g}^j = A^i_{.j}\, \mathbf{g}_i \otimes \mathbf{g}^j \ . \tag{2}$$

In addition, the objective Oldroyd rate of the metric transformation tensor (1)

$$\dot{\mathbf{Q}} = \overset{o}{G}{}^{ik}\, \dot{G}_{kj}\, \mathbf{g}_i \otimes \mathbf{g}^j \tag{3}$$

leads to the definition of the symmetric strain rate

$$\dot{\mathbf{H}} = \frac{1}{2}\, \mathbf{Q}^{-1}\, \dot{\mathbf{Q}} = \frac{1}{2}\, G^{ik} \dot{G}_{kj}\, \mathbf{g}_i \otimes \mathbf{g}^j = \dot{H}^i_{.j}\, \mathbf{g}_i \otimes \mathbf{g}^j \ . \tag{4}$$

The mechanical response of the considered body under loading is governed by different physical mechanisms on micro-, meso- and macroscale levels. Thus, the proposed nonlinear kinematic model accounts for discontinuous fields of dislocation interaction (plastic flow) as well as of microvoid and microcrack interactions (damage growth). Thus, the multiplicative decomposition of the metric transformation tensor [17, 18]

$$\mathbf{Q} = \mathbf{Q}^{pd}\, \mathbf{Q}^{el} \tag{5}$$

into its respective inelastic (plastic and damage) part

$$\mathbf{Q}^{pd} = \overset{o}{G}{}^{ik}\, \overset{*}{G}_{kj}\ \mathbf{g}_i \otimes \mathbf{g}^j \tag{6}$$

and its elastic part

$$\mathbf{Q}^{el} = \overset{*}{G}{}^{ik}\ G_{kj}\, \mathbf{g}_i \otimes \mathbf{g}^j \tag{7}$$

is proposed where the metric $\overset{*}{G}_{ij}$ of the base vectors $\overset{*}{\mathbf{g}}_i$ of the intermediate configuration $\overset{*}{\mathcal{B}}$ has been introduced which represents a fictitious unstressed state at fixed values of internal variables (see Fig. 1).

Experiments have shown that large inelastic strains of ductile materials are accompanied by small or moderate elastic deformations. Therefore, the elastic Almansi strain tensor

$$\mathbf{A}^{el} = \frac{1}{2}\, (\mathbf{1} - \mathbf{Q}^{el-1}) \tag{8}$$

is introduced in its mixed-variant representation as an appropriate elastic strain measure. Based on experimental observations, this tensor (8) is assumed to be kinematically independent from accompanying inelastic deformations. Using the multiplicative decomposition (5), the proposed strain rate tensor (4) is rewritten in the form

$$\dot{\mathbf{H}} = \frac{1}{2}\, \mathbf{Q}^{el-1}\, \mathbf{Q}^{pd-1}\, \dot{\mathbf{Q}}^{pd}\, \mathbf{Q}^{el} \ + \ \frac{1}{2}\, \mathbf{Q}^{el-1}\, \dot{\mathbf{Q}}^{el} \ = \ \dot{\mathbf{H}}^{pd} \ + \ \dot{\mathbf{H}}^{el} \tag{9}$$

which leads to the additive decomposition of the elastic and inelastic strain rates

$$\dot{\mathbf{H}}^{el} = \frac{1}{2}\, \mathbf{Q}^{el-1}\, \dot{\mathbf{Q}}^{el} \tag{10}$$

and

$$\dot{\mathbf{H}}^{pd} = \frac{1}{2}\,\mathbf{Q}^{-1}\,\dot{\mathbf{Q}}^{pd}\,\mathbf{Q}^{el}\,, \tag{11}$$

respectively.

The central idea of the present continuum damage framework is the introduction of specific metric coefficients as appropriate measures of evolving damage. It is based on the introduction of effective undamaged configurations which are obtained by fictitiously removing all the damage the body has undergone and characterize the deformation behavior of the fictitious undamaged material [9, 10, 17, 33, 70, 84, 91]. In particular, the current fictitious configuration $\mathcal{E}$ of the body is obtained from the actual damaged configuration $\mathcal{B}$ by fictitiously removing the damage of the deformed body, see Fig. 1. The corresponding base vectors and metric coefficients of the current undamaged configuration are given by $\mathbf{e}_i$ and $E_{ij} = \mathbf{e}_i \cdot \mathbf{e}_j$, respectively. The initial undamaged configuration $\overset{o}{\mathcal{E}}$ with base vectors $\overset{o}{\mathbf{e}}_i$ and metric coefficients $\overset{o}{E}_{ij} = \overset{o}{\mathbf{e}}_i \cdot \overset{o}{\mathbf{e}}_j$ is obtained by fictitiously removing the initial damage $\overset{o}{\mathcal{B}}$. In addition, the undamaged stress-free intermediate configuration $\overset{*}{\mathcal{E}}$, which corresponds to the intermediate configuration $\overset{*}{\mathcal{B}}$, is characterized by the base vectors $\overset{*}{\mathbf{e}}_i$ and the metric coefficients $\overset{*}{E}_{ij} = \overset{*}{\mathbf{e}}_i \cdot \overset{*}{\mathbf{e}}_j$.

To be able to describe the kinematics of these undamaged configurations, the effective metric transformation tensor [18]

$$\bar{\mathbf{Q}} = \bar{Q}^{i}_{.j}\,\mathbf{g}_i \otimes \mathbf{g}^j = \overset{o}{E}{}^{ik}\, E_{kj}\,\mathbf{g}_i \otimes \mathbf{g}^j \tag{12}$$

is introduced which - similar to the large strain kinematics discussed above - leads to the definition of the corresponding effective logarithmic strain tensor

$$\bar{\mathbf{A}} = \frac{1}{2}\ln\bar{\mathbf{Q}} \tag{13}$$

as well as to the effective strain rate

$$\dot{\bar{\mathbf{H}}} = \frac{1}{2}\,\bar{\mathbf{Q}}^{-1}\,\dot{\bar{\mathbf{Q}}}\,. \tag{14}$$

The multiplicative decomposition of the effective metric transformation tensor

$$\bar{\mathbf{Q}} = \bar{\mathbf{Q}}^{pl}\,\bar{\mathbf{Q}}^{el} \tag{15}$$

leads to its effective plastic part

$$\bar{\mathbf{Q}}^{pl} = \overset{o}{E}{}^{ik}\, \overset{*}{E}_{kj}\;\mathbf{g}_i \otimes \mathbf{g}^j \tag{16}$$

and to its effective elastic part

$$\bar{\mathbf{Q}}^{el} = \overset{*}{E}{}^{ik}\, E_{kj}\,\mathbf{g}_i \otimes \mathbf{g}^j\,. \tag{17}$$

The effective elastic metric transformation tensor $\bar{\mathbf{Q}}^{el}$ describes elastic stretching of the matrix material which is used to introduce the effective elastic Almansi strain tensor

$$\bar{\mathbf{A}}^{el} = \frac{1}{2}\left(\mathbf{1} - \bar{\mathbf{Q}}^{el-1}\right) . \tag{18}$$

The plastic part of the effective metric transformation tensor $\bar{\mathbf{Q}}^{pl}$, on the other hand, is arising from purely irreversible processes due to dislocation motions in the matrix material. In addition, Eqs. (14) and (15) lead to the additive decomposition

$$\dot{\bar{\mathbf{H}}} = \frac{1}{2}\,\bar{\mathbf{Q}}^{el-1}\,\bar{\mathbf{Q}}^{pl-1}\,\dot{\bar{\mathbf{Q}}}^{pl}\,\bar{\mathbf{Q}}^{el} + \frac{1}{2}\,\bar{\mathbf{Q}}^{el-1}\,\dot{\bar{\mathbf{Q}}}^{el} = \dot{\bar{\mathbf{H}}}^{pl} + \dot{\bar{\mathbf{H}}}^{el} , \tag{19}$$

where the effective elastic and plastic strain rate tensors are defined as

$$\dot{\bar{\mathbf{H}}}^{el} = \frac{1}{2}\,\bar{\mathbf{Q}}^{el-1}\,\dot{\bar{\mathbf{Q}}}^{el} , \tag{20}$$

and

$$\dot{\bar{\mathbf{H}}}^{pl} = \frac{1}{2}\,\bar{\mathbf{Q}}^{-1}\,\dot{\bar{\mathbf{Q}}}^{pl}\,\bar{\mathbf{Q}}^{el} , \tag{21}$$

respectively.

Experiments [58] have shown that with increasing plastic deformations damage is initiated in ductile metals and evolves in the continuing deformation process. Additional deformations due to damage are caused by nucleation and isotropic growth of voids as well as by their coalescence and the anisotropic formation of microcracks. To be able to compute damage deformations, the simultaneous motion of the real body and the fictitious undamaged one is considered, and as can be seen from Fig. 1, the second order tensors

$$\overset{o}{\mathbf{R}} = \overset{o}{R}{}^{i}_{.j}\;\mathbf{g}_i \otimes \mathbf{g}^j = \overset{o}{E}{}^{ik}\;\overset{o}{G}_{kj}\;\mathbf{g}_i \otimes \mathbf{g}^j , \tag{22}$$

$$\overset{*}{\mathbf{R}} = \overset{*}{R}{}^{i}_{.j}\;\mathbf{g}_i \otimes \mathbf{g}^j = \overset{*}{E}{}^{ik}\;\overset{*}{G}_{kj}\;\mathbf{g}_i \otimes \mathbf{g}^j \tag{23}$$

and

$$\mathbf{R} = R^{i}_{.j}\,\mathbf{g}_i \otimes \mathbf{g}^j = E^{ik}\,G_{kj}\,\mathbf{g}_i \otimes \mathbf{g}^j \tag{24}$$

are introduced as metric transformation tensors between the respective damaged and undamaged configurations. In particular, the initial damage tensor $\overset{o}{\mathbf{R}}$ characterizes the initial damage state caused, for example, by the process of cold-working, forming or machining of mechanical parts leading to an initial evolution of defects in the virgin material. $\mathbf{R}$ and $\overset{*}{\mathbf{R}}$ represent internal state variables which describe the current general anisotropic damage state of the material. As has been shown in [19], [68], the tensor $\overset{*}{\mathbf{R}}$ characterizes the damage state of the current configuration independently of the current elastic deformation and, thus, accurately describes the reduction

of the material element due to the evolution of microdefects. The relation between the current damage tensors $\mathbf{R}$ and $\overset{*}{\mathbf{R}}$ is given by

$$\mathbf{R} = \bar{\mathbf{Q}}^{el\,-1}\ \overset{*}{\mathbf{R}}\ \mathbf{Q}^{el} \tag{25}$$

(see Fig. 1) and, thus, the metric transformation tensor $\mathbf{Q}$ can be multiplicatively decomposed as

$$\mathbf{Q} = \overset{o}{\mathbf{R}}^{-1}\ \bar{\mathbf{Q}}^{pl}\ \overset{*}{\mathbf{R}}\ \mathbf{Q}^{el}\ . \tag{26}$$

Its completely different physical counterparts are now kinematically decomposed which allows separate formulation of the corresponding constitutive laws. In addition, making use of Eqs. (10), (21), and (26) the strain rate tensor (4) can be rewritten in the form

$$\dot{\mathbf{H}} = \dot{\mathbf{H}}^{el} + \mathbf{R}^{-1}\,\dot{\bar{\mathbf{H}}}^{pl}\,\mathbf{R} + \mathbf{Q}^{el\,-1}\dot{\mathbf{H}}^{da}\,\mathbf{Q}^{el} \tag{27}$$

with the definition of the damage strain rate

$$\dot{\mathbf{H}}^{da} = \frac{1}{2}\,\overset{*}{\mathbf{R}}^{-1}\,\dot{\overset{*}{\mathbf{R}}}\,. \tag{28}$$

Following the fundamental ideas of Gurson [34] and Tvergaard [87] the current damage state is assumed to be adequately characterized by the void volume fraction

$$f = \frac{dv - d\bar{v}}{dv} \tag{29}$$

where dv denotes the differential volume of the current damaged configuration $\mathcal{B}$ and $d\bar{v}$ represents the differential volume of the current undamaged configuration $\mathcal{E}$. A characteristic feature of the proposed continuum damage mechanics framework is that the continuous damage parameter f is directly given by the material geometry on the microscale. Thus, the current value of the damage parameter can be directly determined by the use of microscopy. By contrast, many continuum damage models are based on damage parameters relating to macroscopic material behavior (see [57] for an overview) with no direct relation to the cause of damage on the microlevel. Of course, the proposed continuous measure of damage, f, averages many variables, namely the number of voids, their sizes and shapes, the degree of adhesion between the voids, local variations of void density, local stress concentration effects and so forth, but it is seen to be an adequate phenomenological parameter [8].

Then, the trace of the damage strain tensor is exactly given by [17], [52]

$$\mathrm{tr}\mathbf{A}^{da} = \ln\frac{dv}{d\bar{v}} = \ln(1-f)^{-1} \tag{30}$$

and the isotropic part of the damage strain tensor can be written in the form

$$\mathbf{A}^{da}_{iso} = \frac{1}{3}\ln(1-f)^{-1}\mathbf{1}\ . \tag{31}$$

Taking into account a logarithmic definition of the isotropic damage strains

$$\mathbf{A}^{da}_{iso} = \frac{1}{2}\ln \overset{*}{\mathbf{R}}_{iso} \tag{32}$$

the corresponding spheric part of the damage tensor is expressed as

$$\overset{*}{\mathbf{R}}_{iso} = (1-f)^{-2/3}\mathbf{1} \tag{33}$$

and making use of Eq. (28) one arrives at the isotropic damage strain rate tensor

$$\dot{\mathbf{H}}^{da}_{iso} = \frac{1}{3}(1-f)^{-1}\dot{f}\ \mathbf{1} \tag{34}$$

which describes the increase in volumetric damage strains caused by the isotropic growth of voids. Since an isotropic damage model is only valid in the early damage state, Eqs. (31), (33) and (34) are expected to give a reasonable approximation of the current damage behavior up to a critical porosity f_c indicating the onset of void coalescence leading to highly anisotropic damage processes which will be discussed below. Based on these considerations, Eq. (32) is generalized by the definition of the logarithmic damage strain tensor

$$\mathbf{A}^{da} = \frac{1}{2}\ln \overset{*}{\mathbf{R}} \tag{35}$$

which is assumed to adequately describe the anisotropic damage kinematics of the body.

Moreover, it is assumed that the intermediate and the current undamaged configurations, $\overset{*}{\mathcal{E}}$ and $\mathcal{E}$, are related in the same way as the intermediate and current damaged configurations, $\overset{*}{\mathcal{B}}$ and $\mathcal{B}$ [17], [68]. As a result, these undamaged and damaged configurations are subjected to the identical elastic metric transformation

$$\mathbf{Q}^{el} = \bar{\mathbf{Q}}^{el}\ , \tag{36}$$

which is a common assumption in homogenization theories. This leads to the equivalence of the elastic strain tensors

$$\mathbf{A}^{el} = \frac{1}{2}\left(\mathbf{1} - \mathbf{Q}^{el-1}\right) = \frac{1}{2}\left(\mathbf{1} - \bar{\mathbf{Q}}^{el-1}\right) = \bar{\mathbf{A}}^{el} \tag{37}$$

and the elastic strain rates

$$\dot{\mathbf{H}}^{el} = \dot{\bar{\mathbf{H}}}^{el}\ . \tag{38}$$

3 Constitutive equations

3.1 Definition of stress tensors

Stress measures are introduced considering the damaged and undamaged configurations, respectively, in order to formulate equilibrium equations and constitutive laws. The current macroscopic stress state of the damaged solid is described by the Kirchhoff stress tensor

$$\mathbf{T} = T^{i}_{\cdot j}\,\mathbf{g}_i \otimes \mathbf{g}^j\ . \tag{39}$$

In addition, in the fictitious undamaged configuration the mechanical effect of the Kirchhoff stress tensor $\mathbf{T}$ (39) is characterized by the effective stress tensor

$$\bar{\mathbf{T}}_e = \bar{T}^i_{.j}\, \mathbf{e}_i \otimes \mathbf{e}^j \ . \tag{40}$$

The symmetric tensor $\bar{\mathbf{T}}_e$ is a fictitious stress measure which represents in the matrix material the magnified effect of macroscopic stress caused by damage. Alternatively, the effective stresses can be formulated with respect to the base vectors $\mathbf{g}_i$:

$$\bar{\mathbf{T}} = \bar{T}^i_{.j}\, \mathbf{g}_i \otimes \mathbf{g}^j \ . \tag{41}$$

Furthermore, in any regular material point at time t the stress tensor $\mathbf{T}$ (39) satisfies the equilibrium conditions

$$\mathrm{div}\mathbf{T} + \rho_o \bar{\mathbf{b}} = \mathbf{0} \tag{42}$$

where $\rho_o \bar{\mathbf{b}} = \rho_o \bar{b}_i \mathbf{g}^i$ represents the body forces, ρ_o denotes the initial mass density and div is the divergence operator with respect to the current base vectors $\mathbf{g}_i$.

3.2 Effective undamaged configurations

The effective undamaged configurations are used to formulate the elastic-plastic constitutive equations of the undamaged matrix material [15], [16]. In particular, the rate of the effective specific mechanical work $\dot{\bar{w}}$ is defined by

$$\rho_o\, \dot{\bar{w}} = \bar{\mathbf{T}} \cdot \dot{\bar{\mathbf{H}}} \ . \tag{43}$$

Using Eq. (19), the rate of effective mechanical work (43) can be additively decomposed according to

$$\rho_o\, \dot{\bar{w}} = \rho_o\, \dot{\bar{w}}^{el} + \rho_o\, \dot{\bar{w}}^{pl} = \bar{\mathbf{T}} \cdot \dot{\bar{\mathbf{H}}}^{el} + \bar{\mathbf{T}} \cdot \dot{\bar{\mathbf{H}}}^{pl} \tag{44}$$

into an effective elastic part $\dot{\bar{w}}^{el}$ governed by thermodynamic state equations and an effective plastic part $\dot{\bar{w}}^{pl}$.

The formulation of effective plastic constitutive equations is based on the introduction of plastic internal variables which may be seen as a basic tool to carry forward informations from the microscale (e.g. crystal lattice) to the phenomenological macroscale. Thus, the plastic internal variables determine the hardening behavior of the matrix material. The effective specific free energy $\bar{\phi}$ of the fictitious undamaged configuration is introduced and, since the effective elastic behavior of the matrix material is not influenced by the hardening state, $\bar{\phi}$ is assumed to be additively decomposed into an effective elastic and an effective plastic part

$$\bar{\phi} = \bar{\phi}^{el}(\bar{\mathbf{A}}^{el}) + \bar{\phi}^{pl}(\gamma) \tag{45}$$

where γ denotes the internal mechanical state variable which characterizes the current effective plastic strain state.

Moreover, the second law of thermodynamics can be written in the form

$$\dot{\bar{w}} - \dot{\bar{\phi}} \geq 0 \, . \tag{46}$$

Making use of Eqs. (44) and (45) one arrives at

$$\bar{\mathbf{T}} \cdot \dot{\bar{\mathbf{H}}}^{el} + \bar{\mathbf{T}} \cdot \dot{\bar{\mathbf{H}}}^{pl} - \rho_o \, \frac{\partial \bar{\phi}^{el}}{\partial \bar{\mathbf{A}}^{el}} \cdot \dot{\bar{\mathbf{A}}}^{el} - \rho_o \, \dot{\bar{\phi}}^{pl}(\gamma) \geq 0 \, . \tag{47}$$

Considering non-dissipative processes in the effective elastic range Eq. (47) leads to the relation

$$\bar{\mathbf{T}} \cdot \dot{\bar{\mathbf{H}}}^{el} \; - \; \rho_o \, \frac{\partial \bar{\phi}^{el}}{\partial \bar{\mathbf{A}}^{el}} \cdot \dot{\bar{\mathbf{A}}}^{el} \; = \; 0 \tag{48}$$

governing the strictly reversible deformations. It may be easily shown that the effective elastic strain rate $\dot{\bar{\mathbf{H}}}^{el}$ given by Eq. (20) represents the objective Oldroyd rate of the effective elastic Almansi strain tensor $\bar{\mathbf{A}}^{el}$ which leads to the effective hyperelastic constitutive equation

$$\bar{\mathbf{T}} = \rho_o \, \frac{\partial \bar{\phi}^{el}}{\partial \bar{\mathbf{A}}^{el}} \, . \tag{49}$$

Then Eq. (47) reduces to the effective dissipation function $\bar{D}$:

$$\bar{D} = \bar{\mathbf{T}} \cdot \dot{\bar{\mathbf{H}}}^{pl} - \rho_o \, \dot{\bar{\phi}}^{pl} \geq 0 \, . \tag{50}$$

As a result, the evolution equation for the effective plastic part of the deformation will be formulated in terms of $\dot{\bar{\mathbf{H}}}^{pl}$.

In particular, the finite isotropic effective elastic part of the material behavior is assumed to be governed by the effective Helmholtz free energy function

$$\rho_o \, \bar{\phi}^{el}(\bar{\mathbf{A}}^{el}) = G \; \bar{\mathbf{A}}^{el} \cdot \bar{\mathbf{A}}^{el} + \frac{1}{2}(K - \frac{2}{3}G) \; (\mathrm{tr}\bar{\mathbf{A}}^{el})^2 \tag{51}$$

where G and K represent the shear and bulk modulus of the matrix material, respectively. Taking into account the hyperelastic constitutive relationship (49) the effective stress tensor is expressed in the form

$$\bar{\mathbf{T}} = 2G \; \bar{\mathbf{A}}^{el} + (K - \frac{2}{3}G) \; \mathrm{tr}\bar{\mathbf{A}}^{el} \; \mathbf{1} \, . \tag{52}$$

It has been shown experimentally that the hyperelastic stress-strain law (52) leads to accurate results for a wide class of metals undergoing finite elastic stretches. All strain nonlinearities are incorporated within the nonlinear effective elastic strain tensor $\bar{\mathbf{A}}^{el}$ while the two effective elastic material constants, G and K, are determined from infinitesimal strain experiments.

Furthermore, the onset of plastic yielding is assumed to be governed by the yield condition

$$f^{pl}(\bar{\mathbf{T}}, c) = 0 \tag{53}$$

where c denotes the strength coefficient of the matrix material. Experimental studies on the effect of superimposed hydrostatic pressure on the deformation behavior of metals carried out by Spitzig et al. [83] and Brownrigg et al. [14] have shown that the flow stress depends approximately linearly on hydrostatic pressure. Numerical studies presented by Brünig [16] have elucidated that even small additional hydrostatic stress terms may remarkably effect the onset of localization as well as the associated deformation modes, and that they can lead to a notable decrease in ductility. Hence, plastic yielding of the ductile matrix material is assumed to be adequately described by the yield condition

$$f^{pl}(\bar{I}_1, \bar{J}_2, c) \;=\; \sqrt{\bar{J}_2} \;-\; c\,(1 \;-\; \frac{a}{c}\bar{I}_1) \;=\; 0\;, \tag{54}$$

where $\bar{I}_1 = \mathrm{tr}\bar{\mathbf{T}}$ and $\bar{J}_2 = \frac{1}{2}\,\mathrm{dev}\bar{\mathbf{T}}\cdot\mathrm{dev}\bar{\mathbf{T}}$ are invariants of the effective stress tensor $\bar{\mathbf{T}}$ (41) and a represents the hydrostatic stress coefficient where a/c is a constant material parameter [81].

In addition, an appropriate plastic potential function has to be established in order to develop the desired constitutive equations that accurately describe the mechanical behavior of ductile elastic-plastic materials observed in experiments. The effective plastic strain rate (21) is assumed to be related to the current effective stress tensor through the flow rule which satisfies the positive work dissipation requirements (50). Thus, the plastic potential function $g^{pl}(\bar{\mathbf{T}})$ is also formulated in terms of the effective stress tensor. In elastic-plastically deformed and damaged metals irreversible volumetric strains are mainly caused by damage and, in comparison, volumetric plastic strains are negligible [83]. Therefore, the plastic potential function

$$g^{pl}(\bar{\mathbf{T}}) \;=\; \sqrt{\bar{J}_2} \tag{55}$$

depends only on the second invariant of the effective stress deviator swhich leads to the isochoric effective plastic strain rate

$$\dot{\bar{\mathbf{H}}}^{pl} \;=\; \dot{\lambda}\,\frac{\partial g^{pl}}{\partial \bar{\mathbf{T}}} \;=\; \dot{\lambda}\,\frac{1}{2\sqrt{\bar{J}_2}}\,\mathrm{dev}\bar{\mathbf{T}} \tag{56}$$

where $\dot{\lambda}$ is a non-negative scalar-valued factor. The definition of the normalized deviatoric tensor

$$\bar{\mathbf{N}} \;=\; \frac{1}{\sqrt{2\;\bar{J}_2}}\,\mathrm{dev}\bar{\mathbf{T}} \tag{57}$$

leads to the introduction of the equivalent plastic strain rate

$$\dot{\gamma} \;=\; \bar{\mathbf{N}}\cdot\dot{\bar{\mathbf{H}}}^{pl} \;=\; \frac{1}{\sqrt{2}}\,\dot{\lambda} \tag{58}$$

which is used to express the plastic strain rate tensor (56) in the form

$$\dot{\bar{\mathbf{H}}}^{pl} \;=\; \dot{\gamma}\,\bar{\mathbf{N}}\;. \tag{59}$$

3.3 Anisotropically damaged configurations

The anisotropically damaged configurations are considered to formulate the inelastic constitutive equations of the damaged aggregate. In response of external loading the existence of microdefects results in an increase of the stress level in the remaining effective material and, on the other hand, in a decrease of the stored energy in the damaged material when compared to the response of the virgin undamaged material. This finite elastic-plastic deformation behavior including anisotropic damage is also viewed within the framework of thermodynamics with internal state variables. Taking into account Eq. (28), the rate of the specific mechanical work

$$\rho_o \, \dot{w} = \mathbf{T} \cdot \dot{\mathbf{H}} \tag{60}$$

is additively decomposed:

$$\rho_o \, \dot{w} = \rho_o \, \dot{w}^{el} + \rho_o \, \dot{w}^{pl} + \rho_o \, \dot{w}^{da} = \mathbf{T} \cdot \dot{\mathbf{H}}^{el} + \mathbf{T} \cdot (\mathbf{R}^{-1} \, \dot{\bar{\mathbf{H}}}^{pl} \, \mathbf{R}) + \mathbf{T} \cdot (\mathbf{Q}^{el\,-1} \, \dot{\mathbf{H}}^{da} \, \mathbf{Q}^{el}) \tag{61}$$

into an elastic ($\dot{w}^{el}$), plastic ($\dot{w}^{pl}$) and damage part ($\dot{w}^{da}$), respectively.

The complexity of the continuum model is characterized by the form of the Helmholtz free energy ϕ and by the number of variables. Thus, the definition of ϕ constitutes a crucial point of the formulation since it is the basis for the derivation of the inelastic constitutive equations. The experimentally observed nonlinearities in ductile metal behavior are well documented in the literature and arise from two distinct microstructural changes that take place in the material: one is the plastic flow, the other is the development of microvoids and microcracks. In particular, plastic flow results in permanent deformation and is the consequence of dislocation processes along preferred slip planes which are predominantly controlled by microscopic shear stresses. Since the crystal lattice has been shown to be unaffected during the slip process, the elastic compliances remain insensitive to this mode of microstructural changes. On the other hand, in fully dense materials voids are formed during straining usually by the decohsion or fracture of large inclusions or precipitates and microcracking destroys the band between material grains. It also results in permanent deformation but in contrast to the plastic material behavior it affects the elastic properties. As a consequence, the elastic properties depend on damage variables but not on plastic strains which leads to the assumption of uncoupled elasticity and plasticity. The free energy due to plastic deformations is usually small in comparison with the elastic counterpart and, therefore, the effects of damage on the plastic part will be neglected. In addition, the influence of other state variables on these free energies are assumed to be small. Hence, as has been proposed by Lemaitre [54] and Lu and Chow [61] among others, it is postulated that the energies involved in plastic flow and damage processes are independent. In order to take into account plasticity and damage phenomena in an adequate manner two sets of internal state variables are chosen characterizing formation of dislocations (plastic internal variables) as well as describing nucleation and propagation of microdefects (damage internal variables).

Therefore, it is possible to decouple the Helmholtz free energy into potential functions for each of the internal state variables and coupling is possible in the respective potentials if they

depend on more than one variable. Therefore, the Helmholtz free energy of the damaged material sample is assumed to consist of three parts [19], [20]:

$$\phi = \phi^{el}(\mathbf{A}^{el}, \mathbf{A}^{da}) + \phi^{pl}(\gamma) + \phi^{da}(\mu) \; . \tag{62}$$

The elastic part of the free energy of the damaged material ϕ^{el} is expressed in terms of the elastic and damage strain tensors (8) and (35), whereas the plastic part, ϕ^{pl} due to plastic hardening, and the damaged part, ϕ^{da} due to damage strengthening, only take into account the respective internal effective plastic and damage state variables, γ and μ. Making use of Eqs. (61) and (62) the second law of thermodynamics can be written in the form

$$\begin{aligned} \rho_o \, \dot{w} - \rho_o \, \dot{\phi} \; = \; & \mathbf{T} \cdot \dot{\mathbf{H}}^{el} + (\mathbf{R}\,\mathbf{T}\,\mathbf{R}^{-1}) \cdot \dot{\bar{\mathbf{H}}}^{pl} + (\mathbf{Q}^{el}\,\mathbf{T}\,\mathbf{Q}^{el\,-1}) \cdot \dot{\mathbf{H}}^{da} \\ & - \rho_o \, \frac{\partial \phi^{el}}{\partial \mathbf{A}^{el}} \cdot \dot{\mathbf{A}}^{el} - \rho_o \, \frac{\partial \phi^{el}}{\partial \mathbf{A}^{da}} \cdot \dot{\mathbf{A}}^{da} - \rho_o \, \dot{\phi}^{pl}(\gamma) - \rho_o \, \dot{\phi}^{da}(\mu) \geq 0 \; . \end{aligned} \tag{63}$$

Assuming that the axiom of entropy production holds, the inequality (63) results in the thermodynamic state law

$$\mathbf{T} \; = \; \rho_o \, \frac{\partial \phi^{el}}{\partial \mathbf{A}^{el}} \tag{64}$$

governing strictly reversible deformations where the previously discussed identity of the Oldroyd rates $\dot{\mathbf{H}}^{el} = \dot{\mathbf{A}}^{el}$ has been used. Furthermore, the Clausius-Duhem inequality can be separated into plastic and damage parts

$$(\mathbf{R}\,\mathbf{T}\,\mathbf{R}^{-1}) \cdot \dot{\bar{\mathbf{H}}}^{pl} - \rho_o \, \dot{\phi}^{pl} \geq 0 \tag{65}$$

and

$$\tilde{\mathbf{T}} \cdot \dot{\mathbf{H}}^{da} - \rho_o \, \frac{\partial \phi^{el}}{\partial \mathbf{A}^{da}} \cdot \dot{\mathbf{A}}^{da} - \rho_o \, \dot{\phi}^{da} \geq 0 \; . \tag{66}$$

From Eq. (66) it can be seen that the evolution equation for the damage part of the deformation will be expressed in terms of the damage strain rate $\dot{\mathbf{H}}^{da}$ introduced kinematically by Eq. (28) and the damage condition will be expressed in terms of its work-conjugate stress tensor

$$\tilde{\mathbf{T}} \; = \; \mathbf{Q}^{el}\,\mathbf{T}\,\mathbf{Q}^{el\,-1} \; . \tag{67}$$

Please note that since the plastic potential function ϕ^{pl} with respect to the damaged configuration will not explicitly be formulated the positive plastic work dissipation requirement (65) will not be used in the present framework and, therefore, the plastic strain rate $\dot{\bar{\mathbf{H}}}^{pl}$, which is based on the plastic potential function $\bar{\phi}^{pl}$ with respect to the undamaged configuration, has only to enforce the condition (50). It may be assumed that ϕ^{pl} could be chosen in such a way that the dissipation inequality (65) will always be satisfied. The second dissipation positiveness requirement (66), on the other hand, will be used since the damage elastic and the damage potential functions, ϕ^{el} and ϕ^{da}, will be considered. Equation (66) may also be used to restrict the

possibilities in formulating ϕ^{el} and, especially, may lead to restrictions for material parameters describing elastic deterioration effects.

Moreover, experiments [82] have indicated that the existence of microdefects results in a decrease of the stress level in the aggregate as well as in a decrease of the elastic material properties and of the stored energy in the damaged material when compared to the response of the virgin undamaged material. To be able to describe these phenomena within the constitutive setting of an efficient continuum damage model the elastic strain energy ϕ^{el}, which characterizes the elastic behavior of the damaged aggregate, is chosen to be an isotropic scalar function of the set of its arguments $\mathbf{A}^{el}$ and $\mathbf{A}^{da}$ [19], [35], [62], [69]. Thus, the elastic strain energy function ϕ^{el} is taken to be

$$\rho_o \, \phi^{el}(\mathbf{A}^{el}, \mathbf{A}^{da}) = G \; \mathbf{A}^{el} \cdot \mathbf{A}^{el} + \frac{1}{2}(K - \frac{2}{3}G) \; (\mathrm{tr}\mathbf{A}^{el})^2 + \eta_1 \; \mathrm{tr}\mathbf{A}^{da} \; (\mathrm{tr}\mathbf{A}^{el})^2 + \eta_2 \; \mathrm{tr}\mathbf{A}^{da} \; \mathbf{A}^{el} \cdot \mathbf{A}^{el} + \eta_3 \; \mathrm{tr}\mathbf{A}^{el} \; \mathbf{A}^{da} \cdot \mathbf{A}^{el} + \eta_4 \; \mathbf{A}^{el} \cdot (\mathbf{A}^{el}\mathbf{A}^{da}) \tag{68}$$

where G and K are again the shear and bulk modulus of the undamaged matrix material and $\eta_1, ..., \eta_4$ are material constants which describe the deterioration of the elastic properties by the occurrence of damage. This leads to the Kirchhoff stress tensor (64) of the damaged material

$$\mathbf{T} = 2(G + \eta_2 \; \mathrm{tr}\mathbf{A}^{da}) \; \mathbf{A}^{el} + [(K - \frac{2}{3}G + 2\eta_1 \; \mathrm{tr}\mathbf{A}^{da})\mathrm{tr}\mathbf{A}^{el} + \eta_3 \; (\mathbf{A}^{da} \cdot \mathbf{A}^{el})] \; \mathbf{1} + \eta_3 \; \mathrm{tr}\mathbf{A}^{el}\mathbf{A}^{da} + \eta_4 \; (\mathbf{A}^{el}\mathbf{A}^{da} + \mathbf{A}^{da}\mathbf{A}^{el}) \; . \tag{69}$$

For example, the first and second additional material constants, η_1 and η_2, are related to the isotropic character of damage whereas the third and fourth coefficient, η_3 and η_4, are due to anisotropic evolution of damage. Laboratory investigations on many ductile metals subjected to tensile stresses indicate that principal elastic moduli and the Poisson's ratios decrease as microdefects grow [35], [51, 82]. These experimental observations place the physical bounds on the values of the additional constitutive parameters $\eta_1, ..., \eta_4$ that they have to be taken to be negative.

Furthermore, constitutive equations for damage evolution are required in the proposed framework of continuum damage mechanics. To determine the onset and the continuation of damage the concept of the damage surface is employed in analogy to the yield surface concept of the plasticity theory. However, unlike the yield condition (54) the form of the damage criterion is not well established. For example, Cordebois and Sidoroff [28] among many others employed a damage dissipation potential function formulated in terms of their so-called damage strain energy release rate. In order to overcome certain anomalies associated with the definition of the damage strain energy release rate tensor Chow and Wang [25] formulated a damage dissipation potential in terms of their effective stress tensor. Similarly, the damage condition

$$f^{da}(\tilde{\mathbf{T}}, \sigma) = 0 \tag{70}$$

is here expressed in terms of the stress tensor $\tilde{\mathbf{T}}$ (67), which is work-conjugate to the chosen damage strain rate tensor (28) (see Eq. (66)) and σ denotes the damage threshold which represents the material toughness to microdefect propagation.

In addition, to be able to compute damage strain rates, the damage potential function $g^{da}(\tilde{\mathbf{T}})$ is also formulated in terms of the stress tensor $\tilde{\mathbf{T}}$ providing a realistic physical representation of material degradation. This leads to the damage rule

$$\dot{\mathbf{H}}^{da} = \dot{\mu}\frac{dg^{da}}{d\tilde{\mathbf{T}}} \tag{71}$$

where $\dot{\mu}$ is the rate of the internal damage variable introduced above. The damage rule has to enforce the dissipation inequality (66) which leads to restrictions for the material parameters $\eta_1, ..., \eta_4$ appearing in Eq. (68).

The definition of the damage strain rate tensor (71) requires a damage evolution law which should be determined from realistic damage propagation conditions. Therefore, experimental, theoretical and numerical studies have been performed to understand principal evolution modes of microcracks. Nowadays, it is well known, for example, that voids in structural metals nucleate from larger inclusions soon after the onset of plastic yielding and grow due to plastic deformations of the surrounding matrix material. In addition, void size, void spacing and void distribution may remarkably affect further growth of exising voids and their coalescence [60, 74].

Several authors presented numerical studies and experimental observations on nucleation, growth and coalescence of voids leading to final fracture of tensile bars. For example, micromechanical cell model studies [65, 71, 77] have been used to focus on void nucleation and growth to final failure. They have shown that the rates of growth of long cylindrical and spherical microscopic voids are significantly elevated by the superposition of hydrostatic tensile stresses on a remotely uniform plastic deformation field. The volume changing contribution of void growth is found to remarkably overwhelm the shape changing part when the mean remote normal stress is large. The void enlargement is amplified over the macroscopic strain rate by a factor arising exponentially with the ratio of the mean normal stress to the yield stress. In addition, Mackenzie et al. [63] have shown that the onset of ductile damage in high strength steels strongly depends on the stress triaxiality. Furthermore, fracture by coalescence of voids would be promoted by a high level of triaxiality tension which was found in a series of experiments on notched tensile specimens [36], [37]. Experiments performed by Brownrigg et al. [14] have also shown the dominant effect of hydrostatic stress on nucleation and growth of voids. Since these results suggest a rapidly decreasing fracture ductility with increasing hydrostatic tension, realistic damage criteria must contain a term depending on the first stress invariant, $I_1 = \mathrm{tr}\mathbf{T} = \mathrm{tr}\tilde{\mathbf{T}}$, which may be seen as the dominating factor regulating the rate of nucleation and isotropic growth of voids. Moreover, Tvergaard and Needleman [88] analyzed round tensile bars to investigate the effect of mechanical properties on ductility. They first predicted void formation and nearly isotropic void growth in plastically deformed regions and, after a critical void volume fraction has been passed, the onset of shear deformation with an associated coalescence of voids leading to a microcrack

is observed thus indicating anisotropic damage behavior. These numerical results have been shown to be in good agreement with experimental observations [6], [11]. Hence, provided that the initial void distribution is not too anisotropic, isotropic damage is assumed to characterize the early deformation stage in a realistic manner and the onset of damage is governed by the damage condition

$$f_{iso}^{da} = I_1 - \sigma = 0 \; . \tag{72}$$

In addition, the damage potential function

$$g_{iso}^{da}(\tilde{\mathbf{T}}) = \alpha I_1 \tag{73}$$

leads to the isotropic damage rule

$$\dot{\mathbf{H}}_{iso}^{da} = \dot{\mu} \frac{dg^{da}}{d\tilde{\mathbf{T}}} = \dot{\mu}\alpha \mathbf{1} \tag{74}$$

which in comparison with the kinematically motivated Eq. (34) shows the identities

$$\dot{\mu} = \dot{f} \tag{75}$$

and

$$\alpha = \frac{1}{3}(1-f)^{-1} \; . \tag{76}$$

Equation (75) clearly shows that the rate of the damage internal variable $\dot{\mu}$ represents the void volume fraction rate $\dot{f}$.

Moreover, it is generally agreed that voids typically coalesce through a combination of shearing of the primary inter-void ligaments as well as coalescence of secondary voids across the primary inter-void ligaments also known as void sheeting. This is indicated by the low strain-to-failure values observed in experiments and the sparse population of relatively small voids in the intermediate vicinity of ductile fracture surfaces. Based on experimental observations or finite element analyses on periodically voided ductile metals several authors have proposed values of the critical void volume fraction f_c, which characterizes the onset of coalescence of voids and, thus, of anisotropic damage evolution. Namely, Brown and Embury [13] suggest that two neighboring cavities coalesce when their length has grown to the order of magnitude of their spacing. This local failure mode is a result of development of slip planes in the plastified matrix material between the cavities or simply of necking of the ligament. Their experiments indicate a critical void volume fraction for coalescence of voids of about $f_c = 0.15$ whereas numerical micromechanical analyses presented by Andersson [3] predicted coalescence at $f_c = 0.25$. However, experiments performed by Cialone and Asaro [27] and Moussy [67] have shown that lower void volume fractions were measured in structural alloys near the fracture surface in the center of the neck of round tensile test specimens. Therefore, the critical porosity $f_c = 0.15$ seems to be unrealistically large for real engineering materials.

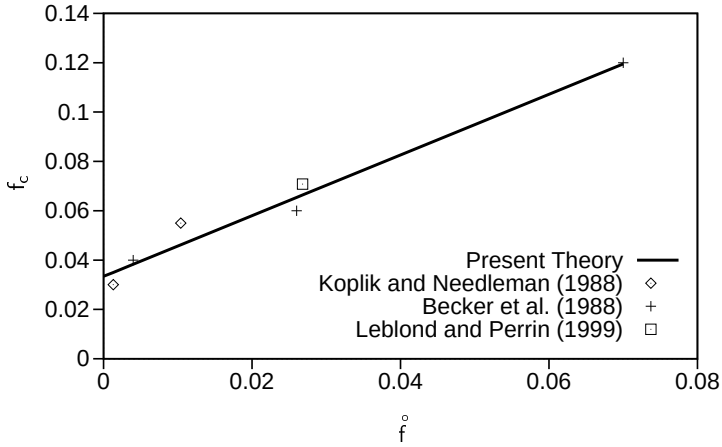

Figure 2: Effect of initial porosity on critical void volume fraction.

The problem of determining the critical porosity f_c through micromechanical finite element simulations taking into account uniform or periodical distribution of voids has also been widely discussed in literature. A large number of numerical calculations, however, yield critical void volume fractions which are quite too large and, thus, lead to an overestimation of the overall ductility. One reason for the discrepancy is the assumed large initial void volume fraction which is not realistic in each case. For example, in engineering alloys voids generally form during straining by the decohesion or fracture of inclusions and, therefore, their initial porosity is very small. Only powder metallurgy consolidated alloys show significant initial porosity.

Numerical cell model studies performed by Becker et al. [6] and Koplik and Needleman [43] indicate that the value of f_c varys slowly with stress triaxiality and matrix strain hardening but to depend strongly on the initial void volume fraction. In addition, numerical calculations reported by Dhar et al. [29] have shown for a wide variation of plastic strains and stress triaxialities that the critical value of damage remains almost the same. Consequently, they regarded their critical damage parameter as a material property for prediction of microcrack initiation in ductile metals. Thus, taking f_c to depend only on the initial void volume fraction $\overset{o}{f}$ may be seen as a reasonable approximation. Then, based on the results of Becker et al. [6], Brünig [19] proposed that the critical void volume fraction f_c of ductile materials depends linearly on the initial porosity $\overset{o}{f}$:

$$f_c = 0.0344 + 1.25 \overset{o}{f} \tag{77}$$

(see Fig. 2). Note that for smaller initial void volume fractions the values of f_c predicted by Eq. (77) are significantly lower than the value $f_c = 0.15$ suggested by Brown and Embury [13] and taken into account by Tvergaard and Needleman [88] within their numerical analyses.

However, one-cell finite element analyses underestimate the observed degradation of strength with increasing porosity due to the stiffness of the regular-array micro-cell model. Real materials normally do not contain periodic but often strongly inhomogeneous distributions of voids. In general, initial voids tend to be gathered in clusters. It is well known that coalescence must start in void clusters much earlier than it would do in a homogeneously voided material. This has been clearly established by Becker [5] based on his numerical study of nonhomogeneously voided solids and also by Thomson et al. [86] using three-dimensional finite element analysis to examine the effect of particle clustering on void damage rates in ductile materials under triaxial loading conditions. Magnusen et al. [64] examined experimentally the contrasting behavior of tensile metal specimens containing random and regular arrays of voids to provide a physical basis for understanding void linking during ductile microvoid fracture. In addition, Dubensky and Koss [30] performed experiments to study the sensitivity of ductile microvoid fracture processes on the size and distribution of voids, and Melander and Stahlberg [66] also analyzed the ductility of materials with different void distributions. Furthermore, Needleman and Kushner [72] and Benson [8] studied numerically the effect of various void distributions on the overall aggregate stress-strain response of initially porous inelastic solids. They found that characterization of a distribution of voids by the continuous void volume fraction f is a reasonable approximation for porous metals. Leblond and Perrin [50] considered several distributions of initial void volume fraction with the same mean value $\overset{o}{f}= 0.0268$ and different standard deviations. Their self-consistent approach based on a model problem with hydrostatic load applied at infinity has shown a decrease of the critical void volume fraction f_c as the standard deviation of the initial void distribution increases. This means that porosity inhomogeneities favor coalescence. For example, the void distribution with the standard deviation of 0.006, which corresponds to actual measurement performed for engineering materials, leads to the critical void volume fraction $f_c = 0.0708$. This result is in good agreement with the critical porosity predicted by Eq. (77) and, therefore, the effect of random nature of experimentally observed void distributions on the critical void volume fraction is also included in the present phenomenological theory. Hence, when the current void volume fraction reaches the critical value $f = f_c$ (Eq. 77), the onset of coalescence of voids is predicted and the damage induced anisotropy caused by the changes in shape of the initially spherical microvoids is assumed to be important and has to be implemented into the present model.

Moreover, Jain et al. [39] compared different criteria to predict the fracture limits of aluminum sheets for a variety of strain ratios. Their numerically predicted forming limit curves have shown that shear-type criteria lead to good agreement with experimental results for different strain paths. Microstructural observations of facture surfaces and through-thickness fracture characteristics confirm a shear-type microvoid coalescence mechanism and subsequent fracture in aluminum sheets. Their qualitative observations show void growth and coalescence as well as the activation of shearing instabilities in the matrix material between the voids in direction of pure shear. Further experiments indicated that a combination of these two damage processes

then leads to final fracture. In addition, Tvergaard and Needleman [88] reported on events during tension of a cylindrical bar. They observed remarkable shear deformation with associated coalescence of voids leading to a microcrack which further grows in a zig-zag fashion. In addition, Le Roy et al. [59] discussed that nucleation and growth of voids were not separable and sequential processes. Voids nucleate continuously during straining and new voids are appearing while older ones are growing. As a result, nucleation and growth should be considered at the same time to be able to realistically describe the evolution of damage with increasing strains. They also have shown that in ductile materials a high deformation value is required to nucleate a significant number of voids and that void nucleation and growth mainly depend on the hydrostatic stress state. Experiments performed by Brownrigg et al. [14] also indicated that the rate of damage was reduced by superimposed hydrostatic pressure whereas later coalescence of voids to oriented microcracks, however, does not depend on hydrostatic stress. Based on these results anisotropic damage behavior of ductile metals is assumed to be adequately described by the damage criterion

$$f^{da}(I_1, J_2, \tilde{\sigma}) = I_1 + \tilde{\beta}\sqrt{\tilde{J}_2} - \tilde{\sigma} = 0 \tag{78}$$

which is also a function of the anisotropic stress measure $\tilde{J}_2 = \frac{1}{2}\mathrm{dev}\tilde{\mathbf{T}} \cdot \mathbb{P}\ \mathrm{dev}\tilde{\mathbf{T}}$ where the anisotropic nature of the problem is characterized by the directional dependence of the projection tensor $\mathbb{P}$. The damage criterion (78) is able to take into account the hydrostatic and deviatoric stress effects caused by the shape and orientation of microdefects, and $\tilde{\sigma}$ denotes the material toughness to microcrack propagation. As long as uniaxial tension tests are used to determine the evolution equation for the equivalent aggregate stress measures σ and $\tilde{\sigma}$ appearing in the damage conditions (72) and (78) the relation $\tilde{\sigma} = (1+\tilde{\beta}/\sqrt{3})\sigma$ holds where σ denotes the uniaxial tension stress. In addition, in Eq. (78) the material property $\tilde{\beta}$ describes the influence of the deviatoric stress state on the damage condition.

Furthermore, the credibility of a damage model is based on how well it correlates with experimental results. For example, it is observed in uniaxial tension tests that microcracks develop perpendicular to the loading direction or the damage is in the direction of loading. Thus, in uniaxial tension damage evolves in the direction of tensile stress. Conversely, in an unconfined uniaxial compressive stress state microcracks develop in the direction parallel to the loading axis. This then corresponds to damage perpendicular to the direction of loading. No stresses are present in this off-axis direction in uniaxial compression but there are tensile deviatoric stresses in the off-axis direction. Based on these observations it appears reasonable to postulate that anisotropic damage evolves in the direction of tensile deviatoric stresses. Therefore, to be able to compute damage strain rates, the damage potential function

$$g^{da}(\tilde{\mathbf{T}}) = \alpha I_1 + \beta\sqrt{\tilde{J}_2} \tag{79}$$

is also formulated in the terms of the stress tensor $\tilde{\mathbf{T}}$ discussed above. In Eq. (79) α and β denote kinematically based damage parameters. Taking into account Eq. (71) this leads to the

nonassociated damage rule

$$\dot{\mathbf{H}}^{da} = \dot{\mu}\alpha\mathbf{1} + \dot{\mu}\beta\frac{1}{2\sqrt{J_2}}\,\mathbb{P}\,\mathrm{dev}\tilde{\mathbf{T}}\;. \tag{80}$$

The first term in Eq. (80) represents the rate of inelastic volumetric deformations caused by the isotropic growth of microvoids whereas the second term is an explicit function of the deviatoric part of its work-conjugate stress tensor to be able to take into account the significant dependence of the evolution of size, shape and orientation of microdefects on the direction of the current stress state.

4 Numerical analyses

4.1 Finite element implementation

In displacement-based finite element procedures usually iterative techniques are employed to solve the discretized nonlinear equilibrium equations for each incremental load or time step. The results of each iteration then correspond to estimates of the incremental displacements from which the current stress and strain states as well as further field variables are computed at the integration points of each finite element. The problem is then to integrate the evolution equations of the respective strain rate tensors over the time increment in order to be able to calculate the current stresses and strains. This is done in the present continuum damage model by the inelastic predictor method presented by Brünig [20] which has been shown to be a stable, accurate and efficient integration algorithm well suited for finite element analyses involving large inelastic deformations.

The finite element procedure is based on the principle of virtual work

$$\int_{B_0} \delta\mathbf{H}\cdot\mathbf{T}\;dv_0 - \int_{\partial B_0} \delta\mathbf{u}\cdot\bar{\mathbf{t}}_0\;da_0 = 0 \tag{81}$$

where B_0 and ∂B_0 denote the volume and surface of the body in the initial configuration and $\delta\mathbf{H} = \frac{1}{2}\mathbf{Q}^{-1}\,\delta\mathbf{Q}$. The first integral in Eq. (81) represents the variation of the current stored energy density while the second accounts for the contribution of the prescribed surface tractions $\bar{\mathbf{t}}_0$.

Using a consistent linearization procedure, choosing suitable shape functions for the unknown displacements, carrying out the integrations and, finally, assembling the individual element stiffness matrices and load vectors, one arrives at a set of linearized algebraic equations for the nodal displacement increments, which may be written in the familiar abbreviated form

$$\mathbf{K}_T\;\Delta\mathbf{V} = \Delta\mathbf{P}\;. \tag{82}$$

In Eq. (82), $\mathbf{K}_T$ denotes the global tangent stiffness matrix, $\Delta\mathbf{P}$ corresponds to the residual unbalanced force vector, and $\Delta\mathbf{V}$ represents the vector of unknown incremental displacements.

4.2 Material characterization

Identification of continuum models consists in the quantitative evaluation of the chosen material coefficients characteristic of each material. The determination of material parameters of the damaged aggregate needs a measurement of damage variables which, however, is somewhat difficult due to the fact that damage does not remarkably affect any measurable quantity far from the rupture condition. Therefore, Spitzig et al. [82] performed a large number of systematic experiments on iron compacts of different initial porosities to provide data that could be used to critically evaluate theoretical models of elastic-plastic behavior of porous ductile solids. They experimentally investigated mechanical properties of iron compacts as well as the effect of deformation on the evolution of void growth characteristics. These experimental data are used to determine the material parameters of the proposed anisotropic continuum damage model.

In particular, taking into account the effective elastic constitutive equation (52) the elastic constants of the iron matrix material are chosen to be the shear modulus G =81300 MPa and the bulk modulus K =166300 MPa. In addition, the effective plastic parameters are estimated using experimental true stress-logarithmic plastic strain curves of fully dense tensile specimens. The nonlinear increase of the current strength coefficient c appearing in the yield condition (54) is numerically characterized by the power law

$$c = c_0 \left(\frac{H_0 \, \gamma}{n \, c_0} + 1 \right)^n \tag{83}$$

to give the best fit to the experimental values. As can be seen from Fig. 3 the numerical simulation based on the initial yield strength $c_0 = 57.74$ MPa, the initial hardening parameter $H_0 = 5500$ MPa, and the hardening exponent $n = 0.296$ leads to good agreement with the experimental curve. In addition, based on the experiments reported by Spitzig and Richmond [81] on the effect of superimposed hydrostatic pressure on the flow characteristics of metals the specific hydrostatic stress coefficient in Eq. (54) is chosen to be $a/c = 23$ TPa^{-1}.

Furthermore, Spitzig et al. [82] measured the current elastic moduli of iron compacts with different porosities. These experimental results are used to determine the material parameters η_1, ..., η_4 in Eq. (69) which describe the deteriorating influence of increasing damage on the elastic properties. As has been shown by Brünig [19] the respective parameters

$$\begin{aligned} \eta_1 &= -117500 \text{ MPa} \,; \quad \eta_2 = -95000 \text{ MPa} \,; \\ \eta_3 &= -190000 \text{ MPa} \,; \quad \eta_4 = -255000 \text{ MPa} \end{aligned} \tag{84}$$

give the best fit to the experimental data. For example, Fig. 4 shows the decrease in Young's modulus, E_d, with increasing void volume fraction. At a current porosity $f = 0.111$, E_d is predicted to attain about 75 % of its initial value, E, and these numerical results agree quite well with the experimental data given in [82]. Similar results may be obtained for the damaged shear modulus, bulk modulus and Poisson's ratio [19]. It should be noted that the decrease in the Poisson's ratio can not be described by standard isotropic as well as a large number of

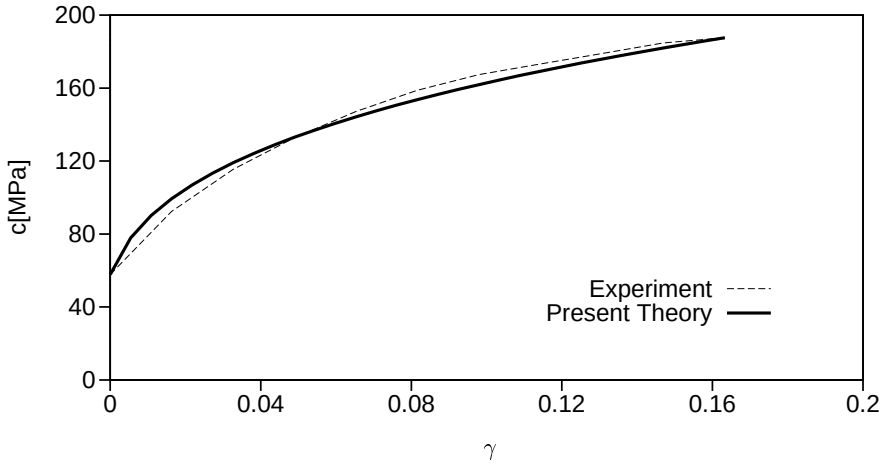

Figure 3: Equivalent matrix stress-equivalent plastic strain curve.

anisotropic damage models [40] whereas the proposed damage approach is even able to simulate this experimentally observed effect [35], [51], [82].

Furthermore, progressive damage often results in strain softening of the aggregate and the corresponding stress-strain curve exhibits a negative slope. Numerical analyses presented by Tvergaard and Needleman [88], for example, suggested that during the increasing damage process the aggregate stress falls slowly until the void volume fraction reaches the critical value $f = f_c$ and, then, the aggregate stress drops abruptly with a remarkable loss of stress carrying capacity. Motivated by these results the equivalent aggregate stress-equivalent damage strain curve is approximated by a bilinear curve where the respective slopes $H^{da} = \frac{d\sigma}{df}$ are chosen to be

$$H_1^{da} = -50 \text{ MPa} \quad \text{for } f < f_c \tag{85}$$

and

$$H_2^{da} = -4000 \text{ MPa} \quad \text{for } f \geq f_c \,, \tag{86}$$

where the critical void volume fraction, f_c, is given by Eq. (77).

The constitutive parameters β and $\tilde{\beta}$ characterizing the portion of anisotropic behavior appearing in the damage rule (80) and the damage condition (78) are chosen to be $\beta = \tilde{\beta} = 0.5$. The effect of different β and $\tilde{\beta}$ on the prediction of deformations of damaged solids has been studied in detail by Brünig [20]. In addition, since no experimental observations on the

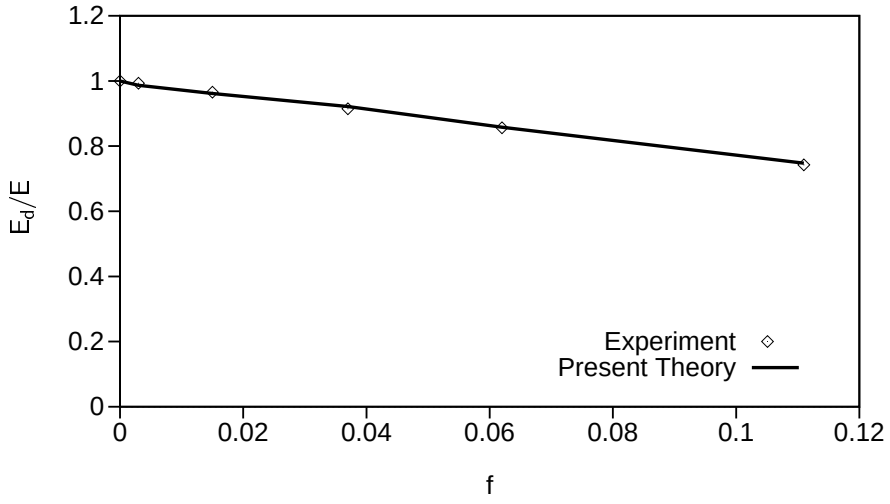

Figure 4: Effect of porosity on Young's modulus.

anisotropic evolution of damage strains are available the principal components of the projection tensor in Eqs. (78) and (80) are taken to be one.

4.3 Tension tests under plane strain conditions

These numerical analyses deal with the finite deformation behavior of uniaxially loaded rectangular specimens with the ratio initial length to initial height of 4. The ends of the bars are taken to be shear free and the specimen has an initial geometric imperfection in shape of a full cosine wave with an amplitude of 1 % of the initial height. Numerical calculations are carried out using displacement-based crossed-triangle elements. They take into account plane strain conditions and employ the elastic-plastic-damage model with the constitutive parameters discussed above. The corresponding load-deflection curves are shown in Fig. 5 based on an elastic-plastic material model without damage, on an elastic-plastic constitutive model including isotropic damage as well as on an elastic-plastic material model including anisotropic damage discussed in this paper. In particular, Fig. 5 shows a remarkable increase in load with increasing deformations due to the initial elastic behavior and the subsequent plastic work-hardening characteristics of the initially undamaged material. The load has a maximum at the elongation $u/l = 0.151$ and subsequently a small decrease in load with increasing deformation is observed due to the decrease in the current specimen's area. In the elastic-plastic case without damage the decrease in load at final elongation $u/l = 0.175$ is only of about 2 %. In addition, Fig. 5 clearly shows that

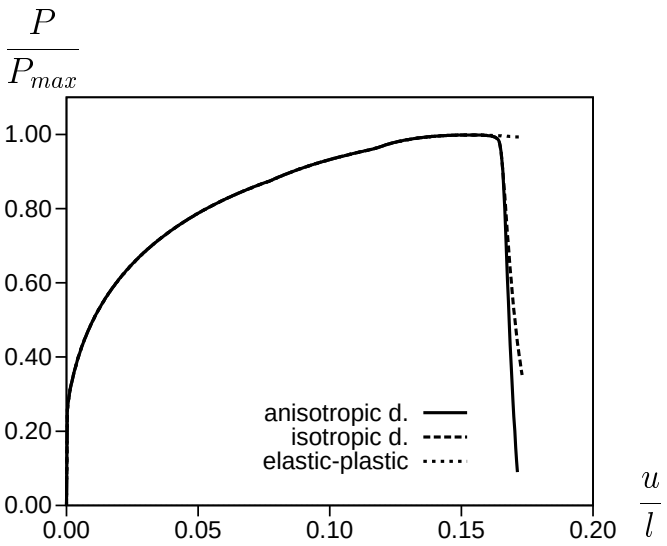

Figure 5: Load-deflection curve.

the numerical calculations based on the proposed damage model predict the onset of damage at the elongation $u/l = 0.162$. The subsequent isotropic damage growth leads to remarkable further decrease in load which at final elongation $u/l = 0.175$ is of about 67 %. Furthermore, the onset of anisotropic damage behavior is predicted at $u/l = 0.167$ and this numerical calculation shows further rapid loss in load carrying capacity with increasing elongation of the specimen. For example, at $u/l = 0.175$ the decrease in load is of about 93 %.

Moreover, Fig. 6 shows the evolution of the void volume fraction f with increasing equivalent plastic strain γ. The numerical calculations predict the onset of isotropic damage at $\gamma = 0.50$ and the isotropic damage model shows an increase in void volume fraction with increasing plastic strain. For example, at $\gamma = 0.70$ the current void volume fraction is $f = 0.15$. The numerical calculation based on the anisotropic damage model, however, predict the onset of anisotropic damage behavior at $\gamma = 0.63$ and shows larger increase in void volume fraction. At $\gamma = 0.70$ the current void volume fraction is of about $f = 0.21$.

Corresponding deformation modes are shown in Fig. 7. The elastic-plastic numerical calculation without damage leads to remarkable necking and large longitudinal strains in the center of the specimen. The numerical calculation based on the isotropic damage model, on the other hand, shows smaller necking behavior and a volume increase in the largely strained elements caused by the isotropic growth of void. This means that in this region the formation of a macro-crack will be initiated which agrees quite well with experimental observations [88]. Similar deformation modes with remarkable volume increases of the center elements are predicted when anisotropic damage behavior is taken into account.

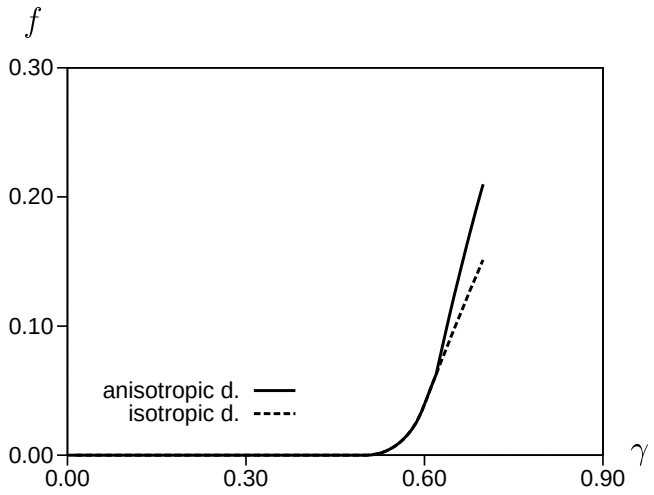

Figure 6: Void volume fraction versus equivalent plastic strain.

5 Conclusions

An anisotropic continuum damage model for ductile metals undergoing progressive plastic deformation induced material deterioration has been discussed. A characteristic feature of the present continuum approach is the kinematic description of anisotropic damage which employs the consideration of damaged as well as fictitious undamaged configurations related via metric transformations which allow for the interpretation of damage tensors. Respective Helmholtz free energy functions of the fictitious undamaged configuration and of the current damaged configuration are introduced separately which allow the formulation of elastic constitutive laws for both the matrix material and the damaged aggregate. Thus, the model does not need strain equivalence, stress equivalence or strain energy equivalence approaches often used in continuum damage theories to be able to connect matrix material and aggregate variables. In contrast to fracture mechanics which considers the process of initiation and growth of microcracks as a discontinuous phenomenon, the proposed continuum damage model uses a continuous variable which is related to the density of the defects in order to describe the deterioration of the material before the initiation of macrocracks. The damage variable is here represented by the void volume fraction and characterizes average material degradation which reflects the various types of damage at the microscale level like nucleation and growth of voids, cavities, microcracks and other microscopic defects.

The applicability of the proposed continuum damage theory is demonstrated by the numerical analyses of the deformation behavior of iron specimens. The phenomenological model is

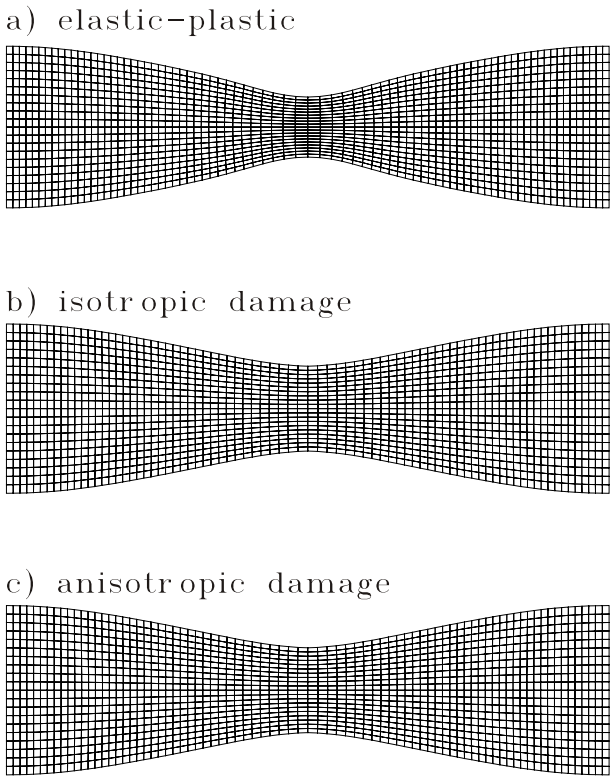

Figure 7: Deformed configurations.

acertained to properly describe the results of the relevant tests. For example, the present approach accurately depicts the deteriorating effect of increasing porosity on elastic moduli and realistically predicts the anisotropic damage evolution of tension specimens. It realistically follows the inception of plastic deformations through the initiation and isotropic growth of voids to void coalescence and the linking up of these voids in microcracks which corresponds to a sudden and remarkable decrease in load carrying capacity of tension specimens. Hence, the present approach deals with the whole damage accumulation process till final fracture. In addition, the proposed continuum damage model may be seen as a powerful basic framework to develop structural models which allow a wide range of practical engineering applications.

References

[1] M. Alves, J. Yu, N. Jones. On the elastic modulus degradation in continuum damage mechanics. Comp. Struct. 76: 703-712, 2000.

[2] M. Alves. Measurement of ductile material damage. Mech. Struct. Mach. 29: 451-476, 2001.

[3] H. Andersson. Analysis of a model for void growth and coalescence ahead of a moving crack tip. J. Mech. Phys. Solids 25: 217-233, 1977.

[4] S. Baste, B. Audoin. On internal variables in anisotropic damage. Eur. J. Mech., A/Solids 10: 587-606, 1991.

[5] R. Becker. The effect of porosity distribution on ductile failure. J. Mech. Phys. Solids 35: 577-599, 1987.

[6] R. Becker, A. Needleman, O. Richmond, V. Tvergaard, Void growth and failure in notched bars. J. Mech. Phys. Solids 36: 317-351, 1988.

[7] W. Becker, D. Gross, A two-dimensional micromechanical model of anisotropic elastic-microplastic damage evolution. Arch. Appl. Mech. (Ingenieur-Archiv) 58: 295-304, 1988.

[8] D.J. Benson. An analysis of void distribution effects on the dynamic growth and coalescence of voids in ductile metals. J. Mech. Phys. Solids 41: 1285-1308, 1993.

[9] J. Betten. Net-stress analysis in creep mechanics. Ingenieur-Archiv 52: 405-419, 1982.

[10] J. Betten. Damage tensors in continuum mechanics. J. Méc. Théor. Appl. 2: 13-32, 1983.

[11] J.I. Bluhm, R.J. Morrissey. Fracture in a tensile specimen. In: Proc. 1st Int. Conf. Fracture, Sendai, Vol. 3: 1739, 1965.

[12] R.J. Bourcier, D.A. Koss, R.E. Smelser, O. Richmond. The influence of porosity on the deformation and fracture of alloys. Acta Metall. 34: 2443-2453, 1986.

[13] L.M. Brown, J.D. Embury. The initiation and growth of voids at second phase particles. In: Proc. 3rd Int. Conf. on Strength of Metals and Alloys, Inst. of Metals, London: 164-169, 1973.

[14] A. Brownrigg, W.A. Spitzig, O. Richmond, D. Teirlinck, J.D. Embury. The influence of hydrostatic pressure on the flow stress and ductility of a spherodized 1045 steel. Acta Metall. 31: 1141-1150, 1983.

[15] M. Brünig. Large strain elastic-plastic theory and nonlinear finite element analysis based on metric transformation tensors. Comput. Mech. 24: 187-196, 1999.

[16] M. Brünig. Numerical simulation of the large elastic-plastic deformation behavior of hydrostatic stress-sensitive solids. Int. J. Plasticity 15: 1237-1264, 1999.

[17] M. Brünig. A framework for large strain elastic-plastic damage mechanics based on metric transformations. Int. J. Eng. Science 39: 1033-1056, 2001.

[18] M. Brünig. Numerical analysis and elastic-plastic deformation behavior of anisotropically damaged solids. Int. J. Plasticity 18: 1237-1270, 2002.

[19] M. Brünig. An anisotropic ductile damage model based on irreversible thermodynamics. Int. J. Plasticity 19: 1679-1713, 2003.

[20] M. Brünig. Numerical analysis of anisotropic ductile continuum damage. Comput. Methods Appl. Mech. Engrg. 192: 2949-2976, 2003.

[21] O.T. Bruhns, P. Schiesse. A continuum model of elastic-plastic materials with anisotropic damage by oriented microvoids. Eur. J. Mech., A/Solids 15: 367-396, 1996.

[22] J.L. Chaboche. Anisotropic creep damage in the framework of continuum damage mechanics. Nuclear Engng. and Design 79: 309-319, 1984.

[23] J.L. Chaboche. Continuum damage mechanics: Part I - General concepts, J. Appl. Mech. 55: 59-64, 1988.

[24] J.L. Chaboche. Continuum damage mechanics: Part II - Damage growth, crack initiation, and crack growth. J. Appl. Mech. 55: 65-72, 1988.

[25] C.L. Chow, J. Wang. An anisotropic theory of continuum damage mechanics for ductile fracture. Eng. Frac. Mech. 27: 547-558, 1987.

[26] C.L. Chow, J. Wang. A finite element analysis of continuum damage mechanics for ductile fracture. Int. J. Fracture 38: 83-102, 1988.

[27] H. Cialone, R.J. Asaro. Hydrogen assisted fracture of spherodized plain carbon steels. Met. Trans. 12A: 1373-1387, 1980.

[28] J.P. Cordebois, F. Sidoroff, Endommagement anisotrope en élasticité et plasticité. Journ. Méc. Théor. Appl. (Num. Spécial): 45-60, 1982.

[29] S. Dhar, R. Sethuraman, P.M. Dixit. A continuum damage mechanics model for void growth and micro crack initiation. Eng. Frac. Mech. 53: 917-928, 1986.

[30] E.M. Dubensky, D.A. Koss. Void/pore distributions and ductile fracture. Metal. Trans A 18A: 1887-1895, 1987.

[31] J. Florez-Lopez. Frame analysis and continuum damage mechanics. Eur. J. Mech., A/Solids 17: 269-283, 1998.

[32] J. Florez-Lopez, A. Benallal, G. Geymonat, R. Billardon. A two-field finite element formulation for elasticity coupled to damage. Comp. Meth. Appl. Mech. Eng. 114: 193-212, 1994.

[33] J. Grabacki. On some desciption of damage processes. Eur. J. Mech., A/Solids 10: 309-325, 1991.

[34] A.L. Gurson. Continuum theory of ductile rupture by void nucleation and growth: Part I - yield criteria and flow rules for porous ductile media. J. Eng. Mat. Tech. 99: 2-15, 1977.

[35] K. Hayakawa, S. Murakami, Y. Liu. An irreversible thermodynamics theory for elastic-plastic-damage materials. Eur. J. Mech., A/Solids 17: 13-32, 1998.

[36] J.W. Hancock, D.K. Brown. On the role of strain and stress state in ductile failure. J. Mech. Phys. Solids 31: 1-24, 1983.

[37] J.W. Hancock, A.C. Mackenzie. On the mechanisms of ductile failure in high strength steels subjected to multiaxial stress-states. J. Mech. Phys. Solids 24: 147-169, 1976.

[38] P. Inglesis, G. Gomez, G. Quintero, J. Florez-Lopez. Model of damage for steel frame members. Eng. Struct. 21: 954-964, 1999.

[39] M. Jain, J. Allin, D.J. Lloyd. Fracture limit prediction using ductile fracture criteria for forming of an automotive aluminum sheet. Int. J. Mech. Sci. 41: 1273-1288, 1999.

[40] J.W. Ju. Isotropic and anisotropic damage variables in continuum damage mechanics. J. Eng. Mech. 116: 2764-2770, 1990.

[41] L.M. Kachanov. On rupture time under condition of creep. Izvestia Akademi Nauk USSR, Otd. Techn. Nauk, Moskwa 8: 26-31, 1958.

[42] M. Kachanov. Continuum model of medium with cracks. J. Eng. Mech. Div. 106: 1039-1051, 1980.

[43] J. Koplik, A. Needleman. Void growth and coalescence in porous plastic solids. Int. J. Solids Structures 24: 835-853, 1988.

[44] D. Krajcinovic. Constitutive equations for damaging materials. J. Appl. Mech. 50: 355-360, 1983.

[45] D. Krajcinovic. Continuous damage mechanics revisted: Basic concepts and definitions. Journ. Appl. Mech. 52: 829-834, 1985.

[46] D. Krajcinovic. Damage mechanics. Mech. Mater. 8: 117-197, 1989.

[47] D. Krajcinovic, M. Basista, D. Sumarac. Micromechanically inspired phenomenological damage model. Journ. Appl. Mech. 58: 305-310, 1991.

[48] D. Krajcinovic, G.U. Fonseka. The continuous damage theory of brittle materials. Part 1: General theory, J. Appl. Mech. 48: 809-815, 1981.

[49] D. Krajcinovic, G.U. Fonseka. The continuous damage theory of brittle materials. Part 2: Uniaxial and plane response modes, J. Appl. Mech. 48: 816-824, 1981.

[50] J.-B. Leblond, G. Perrin. A self-consistent approach to coalescence of cavities in inhomogeneously voided ductile solids. J. Mech. Phys. Solids 47: 1823-1841, 1999.

[51] H. Lee, K. Peng, J. Wang. An anisotropic damage criterion for deformation instability and its application to forming limit analysis of metal plates. Eng. Frac. Mech. 21: 1031-1054, 1985.

[52] Th. Lehmann. Some thermodynamical considerations on inelastic deformations including damage processes. Acta Mech. 79: 1-24, 1989.

[53] Th. Lehmann. Thermodynamical foundations of large inelastic deformations of solid bodies including damage. Int. J. Plasticity 7: 79-98, 1991.

[54] J. Lemaitre. A continuous damage mechanics model for ductile fracture. J. Eng. Mater. Tech. 107: 83-89, 1985.

[55] J. Lemaitre. Coupled elasto-plasticity and damage constitutive equations. Comp. Meth. Appl. Mech. Eng. 51: 31-49, 1985.

[56] J. Lemaitre. Local approach of fracture. Eng. Frac. Mech. 25: 523-537, 1986.

[57] J. Lemaitre. A course on damage mechanics. Springer, Berlin, 2nd ed. , 1996.

[58] J. Lemaitre, J. Dufailly. Damage measurements. Eng. Frac. Mech. 28: 643-661, 1987.

[59] G. Le Roy, J.D. Embury, G. Edward, M.F. Ashby. A model of ductile fracture based on the nucleation and growth of voids. Acta Metall. 29: 1509-1522, 1981.

[60] Z. Li, C. Wang, C. Chen. The evolution of voids in the plasticity strain hardening gradient materials. Int. J. Plasticity 19: 213-234, 2003.

[61] T.J. Lu, C.L. Chow. On constitutive equations of inelastic solids with anisotropic damage. Theor. Appl. Fract. Mech. 14: 187-218, 1990.

[62] V.A. Lubarda, D. Krajcinovic. Some fundamental issues in rate theory of damage-elastoplasticity. Int. J. Plasticity 11: 763-797, 1995.

[63] A.C. Mackenzie, J.W. Hancock, D.K. Brown. On the influence of state of stress on ductile failure initiation in high strength steels. Eng. Frac. Mech. 9: 167-188, 1977.

[64] P.E. Magnusen, E.M. Dubensky, D.A. Koss. The effect of void arrays on void linking during ductile fracture. Acta Metall. 36: 1503-1509, 1988.

[65] F.A. McClintock. A criterion for ductile fracture by growth of holes. Journ. Appl. Mech. 35: 363-371, 1968.

[66] A.Melander, U. Stahlberg. The effect of void size and distribution on ductile fracture. Int. J. Fracture 16: 431-440, 1980.

[67] F. Moussy. Les differentes echelles du developpement de l'endommagement dans del aciers. Influence sur la localization de la deformation a l'echelle microscopique. In: Salencon, J. (ed.), Proc. Int. Symp. on Plastic Instability – Considere Memorial, Presses Ponts et Chaussees: 263-272, 1985.

[68] S. Murakami. Mechanical modeling of material damage. J. Appl. Mech. 55: 280-286, 1988.

[69] S. Murakami, K. Kamiya, Constitutive and damage evolution equations of elastic-brittle materials based on irreversible thermodynamics. Int. J. Mech. Sci. 39: 473-486 (1997).

[70] S. Murakami, N. Ohno. A continuum theory of creep and creep damage, in: Ponter, A.R.S., Hayhurst, D.R., Eds., Creep in Structures (Springer Verlag, Berlin, 1981): 422-443, 1981.

[71] A. Needleman. Void growth in an elastic-plastic medium. J. Appl. Mech. 41: 964-970, 1972.

[72] A. Needleman, A.S. Kushner. An analysis of void distribution effects on plastic flow in porous solids. Eur. J. Mech., A/Solids 9: 193-206, 1990.

[73] E.T. Onat, F.A. Leckie, Representation of mechanical behavior in the presence of changing internal structure. Journ. Appl. Mech. 55: 1-10, 1988.

[74] V.C. Orsini, M.A. Zikry. Void growth and interaction in crystalline materials. Int. J. Plasticity 17: 1393-1417, 2001.

[75] M. Ortiz. A constitutive theory for the inelastic behavior of concrete. Mech. Mater. 4: 67-93, 1985.

[76] I.N. Rabotnov. On the equations of state for creep, in: Progress in Appl. Mech. - The Prager anniversary volume (MacMillan, New York, 1963): 307-315, 1963.

[77] J.R. Rice, D.M. Tracey. On the ductile enlargement of voids in triaxial stress fields. J. Mech. Phys. Solids 17: 201-217, 1969.

[78] G. Rousselier, Ductile fracture models and their potential in local approach of fracture. Nucl. Eng. Design 105: 97-111, 1987.

[79] J.C. Simo, J.W. Ju. Strain- and stress-based continuum damage models - I. Formulation. Int. J. Solids Struct. 23: 821-840, 1987.

[80] J.C. Simo, J.W. Ju. Strain- and stress-based continuum damage models - II. Computational aspects. Int. J. Solids Struct. 23: 841-869, 1987.

[81] W.A. Spitzig, O. Richmond. The effect of pressure on the flow stress of metals, Acta Metall. 32: 457-463, 1984.

[82] W.A. Spitzig, R.E. Smelser, O. Richmond. The evolution of damage and fracture in iron compacts with various initial porosities. Acta Metall. 36: 1201-1211, 1988.

[83] W.A. Spitzig, R.J. Sober, O. Richmond. Pressure dependence of yielding and associated volume expansion in tempered martensite. Acta Metall 23: 885-893, 1975.

[84] P. Steinmann, I. Carol. A framework for geometrically nonlinear continuum damage mechanics. Int. J. Eng. Science 36: 1793-1814, 1998.

[85] W.H. Tai, B.X. Yang, A new microvoid-damage model for ductile fracture. Eng. Frac. Mech. 25: 377-384, 1986.

[86] C.I.A. Thomson, M.J. Worswick, A.K. Pilkey, D.J. Lloyd. Void coalescence within periodic clusters of particles. J. Mech. Phys. Solids 51: 127-146, 2003.

[87] V. Tvergaard. Material failure by void growth to coalescence. Adv. Appl. Mech. 27: 83-151, 1990.

[88] V. Tvergaard, A. Needleman. Analysis of the cup-cone fracture in a round tensile bar. Acta Metall. 32: 157-169, 1984.

[89] G.Z. Voyiadjis, P.I. Kattan. A plasticity-damage theory for large deformation of solids - I. Theoretical formulation. Int. J. Eng. Science 30: 1089-1108, 1992.

[90] G.Z. Voyiadjis, P.I. Kattan. Advances in Damage Mechanics: Metals and Metal Matrix Composites. Elsevier, Amsterdam. , 1999.

[91] G.Z. Voyiadjis, T. Park. The kinematics of damage for finite-strain elasto-plastic solids. Int. J. Eng. Science 37: 803-830, 1999.